Research Square

Preprints are preliminary reports that have not undergone peer review.
They should not be considered conclusive, used to inform clinical practice,
or referenced by the media as validated information.

Adaptive Strategies and Resistome Dynamics of Microbial Communities in an Intensive Care Unit

Shijiao Qi
Xi'an Jiaotong-Liverpool University
Lining Huang
The Affiliated Suzhou Hospital of Nanjing Medical University
Xia Huang
Xi'an Jiaotong-Liverpool University
Li Sun
Xi'an Jiaotong-Liverpool University
Shenglun Chen
Xi'an Jiaotong-Liverpool University
Zhiming Qiao
The Affiliated Suzhou Hospital of Nanjing Medical University
Xinzhao Tong
xinzhao.tong@xjtlu.edu.cn

Xi'an Jiaotong-Liverpool University

Research Article

Keywords: Intensive care unit, adaptive strategies, pathogenic microbes, resistance genes, horizontal gene transfer, mobile genetic elements, intrinsic genetic modification

Posted Date: May 26th, 2026

DOI: https://doi.org/10.21203/rs.3.rs-9376613/v1

License: This work is licensed under a Creative Commons Attribution 4.0 International License.
Read Full License

Additional Declarations: No competing interests reported.

Abstract

Background

In clinical environments, rigorous and frequent sanitation regimes are fundamental to infection control. These persistent hygiene practices create a unique selective landscape that may shape the functional traits and resistance of the indoor microorganisms. To explore the adaptive mechanisms of microbes in this high-pressure environment, particularly those that are associated with hospital-acquired infection (HAI), we conducted a longitudinal metagenomic study in an intensive care unit (ICU). By characterizing the microbial communities on hospital surfaces and nurses' hands over a six-month period, we aimed to elucidate the metabolic strategies and resistome dynamics that facilitate microbial persistence in the clinical setting.

Results

Our findings revealed that opportunistic pathogens such as *Staphylococcus epidermidis*, *Micrococcus luteus*, and *Corynebacterium striatum* were consistently abundant and persistent in the ICU environment, with some exhibiting high metabolic activity and a potential to thrive. The dispersal of pathogenic microbes from the nurse's hand to the ICU surfaces was generally limited and primarily mediated by a neutral process. Following genome assembly and dereplication, we recovered 38 representative metagenomic-assembled genomes (rMAGs) that could be classified only at the genus level or higher, indicating their novelty. Functional analysis revealed that novel genomes, notably belonging to the genus *Pseudomonas*, harbored a large number of high-risk antimicrobial resistance genes (ARGs) that confer resistance to multiple compounds, including antibiotics, biocides, and heavy metals. The presence of these ARGs in known pathogens and novel genomes may result from horizontal gene transfer (HGT), mediated by mobile genetic elements (MGEs) including plasmids, phages, and phage–plasmid hybrids. Beyond this, a few novel genomes also exhibited intrinsic genetic modifications, including the amplification of genes associated with biofilm formation, multidrug efflux, and stress tolerance, which may serve as strategies for adapting to persistent environmental pressures in clinical settings.

Conclusions

Despite stringent sanitization, opportunistic pathogens and taxa of unknown pathogenicity persist in ICU environments through specialized adaptive strategies that use HGT and intrinsic genetic modifications to drive resistance development under clinical environmental stress. These findings underscore the importance of monitoring microbial evolution and the persistence mechanism in high-pressure clinical niches.

Introduction

Multidrug-resistant (MDR) microorganisms are a major contributor to healthcare-associated infections (HAIs), affecting an estimated 5–15% of hospitalized patients annually [1]. Within intensive care units (ICUs), the incidence of HAIs can even exceed 30% [2], posing severe threats to immunocompromised patients. These resistant microorganisms can be consistently seeded from infected patients to nearby surfaces and further disseminate within hospital environments through skin-surface contact. Healthcare workers serve as mobile vectors of infection, particularly during healthcare-related procedures, when medical devices and high-touch hospital surfaces act as persistent reservoirs and transmission hubs [3, 4].

To mitigate HAIs, healthcare facilities routinely implement rigorous, high-frequent sanitization protocols. While these practices are essential for infection control, they create a unique anthropogenic selective landscape. The constant application of antimicrobial agents, ranging from oxidizing agents to membrane-disrupting compounds, imposes significant survival pressure on the indoor microbiota [5]. Emerging evidence suggests that the clinical environment may select for specific functional traits that facilitate the persistence of pathogenic microbes. For instance, *Staphylococcus aureus* strains isolated from ICU surfaces have demonstrated greater tolerance to common clinical cleaning agents like benzalkonium chloride (BAC), genetically supported by the presence of efflux pump genes, such as *qacA* and *qacE* [6].

Beyond specific resistance genes, the collective pressures of the clinical environment may drive broader adaptive strategies through two interconnected pathways: enhanced intrinsic tolerance and facilitated horizontal gene transfer (HGT). First, the high-pressure clinical niches select for mutations that rewire core cellular systems, such as multidrug efflux, membrane permeability, and global transcription [6]. These modifications often result in a “cross-resistance” phenotype, where adaptation to environmental stressors simultaneously confers resistance to antibiotics [6]. This trajectory is frequently linked to enhanced biofilm formation, a key persistence phenotype that shields microbial communities from both chemical stress and desiccation [7]. Second, the clinical environment may mechanically accelerate the exchange of antimicrobial resistance genes (ARGs). Selective pressures [8] increase the extracellular pool of ARGs or induce stress responses that promote the uptake of ARG-carrying mobile genetic elements by competent bacteria [8]. Consequently, the structured, high-density biofilm environment is highly conducive to conjugative plasmid transfer, potentially amplifying the spread of multidrug resistance within hospital environments [9].

While these observations underscore the potential for clinical practices to shape microbial evolution, there remains a paucity of longitudinal field studies evaluating how the high-pressure ICU environment influences the adaptive strategies of entire microbial communities in real-world settings. To bridge this gap, we conducted a six-month longitudinal study in an ICU of the Affiliated Suzhou Hospital of Nanjing Medical University. Samples were swabbed from high-touch indoor surfaces and nurses’ hands after routine disinfection, and then subjected to shotgun metagenomic sequencing. We aimed to characterize the spatiotemporal dynamics of pathogens and their transmission potential between healthcare workers and the clinical environments. In addition, we aimed to characterize ARGs in pathogenic microbes and

their potential for inter-species exchange through HGT to infer the adaptive metabolic strategies microbes use to persist in this niche. Finally, we employed comparative genomics to examine resistance-associated mutations in species-level unclassified bacterial genomes, aiming to elucidate the evolutionary trajectories that enable novel taxa to adapt in the ICU setting. This study provides novel insights into the microbial adaptation within clinical environments, which will contribute to more robust infection prevention and antimicrobial stewardship practices.

Method

Sample collection and shotgun metagenomic sequencing

A total of 77 samples were systematically collected from the ICU ward of the Hepatobiliary Surgery Department at the Affiliated Suzhou Hospital of Nanjing Medical University. This particular department was selected due to its documented high incidence of HAIs, a phenomenon attributed to the frequent necessity of invasive surgical procedures. Such interventions inevitably create extensive interfaces for patient exposure to nosocomial pathogens, including antibiotic-resistant strains prevalent within the hospital environments. Environmental sampling was performed across five predefined sites within the ICU. These included the outer surfaces of respiratory masks (sourced from fixed-bed locations), bed rails, call buttons, and computer mouse surfaces. The rationale for selecting the first four surface types was their frequent contact with healthcare workers' hands, which can serve as potential fomites for pathogen transmission. The inner surface of the ICU entrance door, conversely, was chosen as a control site due to its minimal direct contact. In addition, to assess human carriage of microorganisms, skin samples were collected from the left and right hands of the on-duty nurses on each sampling day.

The methodology for sample collection spanned six months, from March to August 2023. This was meticulously designed across four distinct phases to capture temporal variations: an initial phase of weekly sampling over five consecutive weeks, followed by biweekly sampling across two months, and concluding with single monthly and bimonthly sampling time points (Fig. 1a). All samples were consistently collected on Thursdays from predefined sites after surface disinfection to minimize temporal variability, ensuring methodological rigor throughout the study.

For sample processing, sterile swabs were used to collect samples by swabbing each predefined surface for 60 seconds. Immediately after collection, each swab was placed into a tube containing DNA stabilization buffer (DNA/RNA Shield™, Zymo Research, United States) to preserve nucleic acid integrity while inactivating any infectious agents. Negative controls, consisting of two unused blank swabs, were processed in the same manner as actual samples. Total DNA was extracted using the QIAGEN® DNeasy PowerSoil Pro kit, following the manufacturer's protocol. The extracted genomic DNA (gDNA) was then sent to 3D Medicines (Shanghai, China) for library preparation using Roche® KAPA HyperPrep Kits explicitly designed for low-biomass samples. Finally, the prepared libraries were sequenced on an Illumina Novaseq 6000 sequencing platform, generating a minimum of 15 Gbp of 150-bp paired-end reads per sample.

Quality control of sequence reads

The initial quality of raw sequences was checked using FastQC. The residual adapter sequences in raw reads were subsequently removed using AdapterRemoval (v2.3.2) [10]. To infer potential contaminations, short reads from the quality-filtered negative controls were co-assembled into contigs, each with a minimum length of 1000 bp, using MEGAHIT (v1.2.9) [11]. The generated contig files and the human reference genome hg37 were used as the self-curated and standard human reference databases, respectively. Any sequences within the samples that mapped to these reference databases were subsequently removed using KneadData (https://github.com/biobakery/biobakery/wiki/kneaddata, v0.12.0) with default parameters. The resulting clean unpaired reads were further deleted using fastq-pair (https://github.com/linsalrob/fastq-pair), generating paired-end ".fastq" files for all downstream bioinformatics analyses [11].

Evaluation of low-biomass sample processing workflow using microbial mock community

To evaluate the accuracy of the entire workflow, particularly for the low-biomass samples in this study, positive controls were included. These consisted of a series of dilutions (0.5, 1, 5, 10, and 25 ng total mass) of gDNA extracted from the ZymoBIOMICS® Microbial Community Standard (Zymo Research, United States). This mock community consists of eight bacterial species, each with a theoretical relative abundance of 12%, and two fungal species, each with a theoretical relative abundance of 2%. The annotated taxonomic information of these positive controls was calculated at the species level. The known theoretical relative abundances were then directly compared with those derived from the clean sequences of the mock community, providing a robust assessment of library preparation and sequencing accuracy. The result showed that the total mass of gDNA did not alter the mock community's overall microbial composition. However, we observed deviations from theoretical values for some species, likely due to species-specific biases during gDNA extraction. Despite this, the library preparation and sequencing protocols successfully detected microbes in the low-biomass samples, demonstrating their high sensitivity (**Fig. S1**).

Taxonomic classification and diversity analysis

Following quality control and filtering, the clean paired-end reads were subjected to taxonomic annotation using Kraken2 (v2.1.1) [12] against the PlusPFP database (June 2024 version), with the parameter "–report-zero-counts" enabled to ensure comprehensive reporting. To correct the underestimation in species-level assignment by the lowest common ancestor applied in Kraken2, the species-level abundance was adjusted by Bracken (v2.5) [13].

Community-level analyses were conducted using the R platform (v4.4.0). For alpha-diversity analysis, all samples were rarefied to a depth of one million reads using the "rarefy" function from the R "vegan"

package (v2.6-10). Ten samples with insufficient reads were excluded. Alpha-diversity metrics, namely Pielou's evenness, richness (i.e., species number), and the abundance-based Shannon diversity index, were calculated for the rarefied species-level taxonomic table using the function "diversity" in the R package "vegan". Differences in alpha-diversity across sampling sites were assessed using the Kruskal-Wallis test. Pairwise comparisons were conducted with Dunn's test, followed by Benjamini-Hochberg (BH) correction to control for false discovery rate.

Linear Discriminant Analysis (LDA) was conducted using the R "MASS" package (v7.3-65) to evaluate differences in microbial community composition across seven sampling sites over multiple sampling dates. Additionally, Permutational Multivariate Analysis of Variance (PERMANOVA) was applied to assess the significance of sampling variables, specifically sampling time and sampling location, on the microbial community structure. This analysis was conducted using the "adonis2" function from the R "vegan" package, with the "by=margin" parameter to evaluate the contribution of each factor separately. To assess the assumption of homogeneity of multivariate dispersions underlying PERMANOVA, Permutational Analysis of Multivariate Dispersions (PERMDISP) was conducted using the "betadisper" function in the "vegan" package to evaluate differences in within-group multivariate dispersion among sample groups.

Pathogen inference and transmission prediction

Kraken2-based species-level annotations were compared with the gcPathogen database [14] to identify known pathogens and their biosafety levels. To evaluate the potential for hand-mediated surface microbial dispersal, the Sloan neutral community model [15] was applied with nurse skin samples as the source and five clinical surface samples as sinks. The model fit was assessed using a Poisson-based approach to quantify the probability of taxon occurrence under neutral assumptions. All statistical analyses, model fitting, and prediction were performed in R.

MAG reconstruction, abundance quantification, and growth rate inference

To infer genome-level information, the clean short reads from the surface and skin samples collected on the same date were co-assembled using MEGAHIT (v1.2.9) [11] with a minimum contig length of 1000 bp. The co-assembled contigs were then binned into metagenome-assembled genomes **(**MAGs) using the MetaWRAP "binning" module with three different binning algorithms (i.e., metaBAT2, MaxBin2, and CONCOCT) [16]. The resulting MAGs were refined using the MetaWRAP "bin_refinement" module with thresholds of completeness ≥ 50% and contamination ≤ 10%, and further dereplicated using dRep (v.3.0.0) [17] with an average nucleotide identity (ANI) of 99%, therefore generating 180 representative MAGs (rMAGs). These rMAGs were taxonomically annotated using CAT/BAT/RAT (v.2.1.0) [18] based on the GTDB database [19], and those associated with pathogenic species were identified using the gcPathogen database [14].

The abundances of each rMAG across individual samples were calculated as transcripts per million (TPM) by coverM (v 0.7.0) with a minimum read identity of 95% and a minimum aligned length of 75% [20]. The *in situ* replication activity of rMAGs was inferred using GRiD (Growth Rate InDex, v1.3). Values below 1.5 were interpreted as indicative of generally slow-growing populations, whereas rMAGs with mean GRiD values ≥ 1.5 across all sampling dates were defined as actively growing taxa, based on the interpretation framework of the original GRiD study [21].

Risk assessment of ARGs carried by rMAGs

Prodigal (v1.14.6) was then used to identify open reading frames (ORFs) from the rMAGs, including their amino acid and nucleic acid sequences, using the parameter "-p meta". The identification of ARGs was performed using BLASTp against the MEGARes database [22], with an E-value ≤ 10 − 5, an identity ≥ 80%, and a coverage ≥ 80% [23]. According to the framework established by Zhang *et al*. [24], the risk index (RI) of ARGs was calculated based on four key parameters: human accessibility, mobility, pathogenicity, and clinical relevance. Based on the RI values, ARGs were classified into four categories: Q1 (highest risk, top 25% of RI values), Q2 (50–75%), Q3 (25–50%), and Q4 (lowest risk, bottom 25%). ARGs in Q1 are often associated with multidrug resistance and are typically found in highly pathogenic microorganisms (e.g., ESKAPE pathogens), showing strong transmission potential among human populations. Q2 ARGs, while posing a significant health threat, are more commonly found in pathogenic microorganisms that primarily infect high-risk populations, such as immunocompromised patients and the aging population. ARGs in Q3 and Q4 present lower transmission risks, as they are usually found in natural environments with limited human exposure and generally confer resistance to a single antibiotic, thus posing a relatively minor public health threat. In this study, ARGs assigned to Q1 and Q2 categories were defined as high-risk ARGs due to their elevated potential for human exposure and clinical impact. All remaining ARGs, including those in Q3, Q4, and the no-risk group, were collectively categorized as low-risk for health hazard evaluation.

Determination of viruses

Contigs (> 1000 bp) were clustered using VAMB (v.4.1.3) [25] based on *k*-mer composition and abundance profiles. Viral bins were identified using PHAMB (v.1.0.1) [26] and their quality assessed using CheckV (v1.0.1; database v0.6) [27] with the "end_to_end" pipeline. All viral bins with completeness ≥ 50% were clustered into species-level vOTUs using a 95% ANI threshold and a minimum coverage of 85%, with centroid-based clustering [28]. To identify proviruses in rMAGs, PHASTER (https://phaster.ca/) was used [29]. ORFs within the vOTUs and proviruses were predicted using Prodigal (v1.14.6) [30] with the "-p meta" parameter.

Identification of plasmids and phage-plasmid elements

Plasmid sequences in rMAGs were identified by geNomad (v1.8.0) [31] with default parameters. The distinct plasmids were defined as those with nucleotide identity < 80% and pairwise alignment coverage < 80% [32]. The replicon and relaxase typing of the plasmid was identified by MOB-suite (v.3.0.0) with the function “mob_typer” [33]. To explore the phylogenetic relationship of the Direct Terminal Repeat (DTR)-associated plasmid contig in a *Staphylococcus hominis* rMAG (330_bin.11), a local BLASTn search was performed against the NCBI plasmid database. Sequences with ≥ 95% identity and ≥ 90% coverage were retained for further analysis. Multiple sequence alignment was carried out using MAFFT (v7.525) [34] with the “--auto" option, followed by alignment trimming with trimAl (v1.5.0) [35] using the “-automated1” parameter. A maximum-likelihood phylogenetic tree was constructed with FastTree (v2.1.11) [36] and then visualized using iTOL [37].

To identify potential phage-plasmid elements, the mined phage sequences were retained, with genome lengths ranging from 10 to 300 kb [38]. Subsequently, a BLAST comparison was performed between the retained phage genomes and the identified plasmid sequences. A phage sequence was defined as a phage-plasmid if it exhibited a BLAST hit against a plasmid sequence that satisfied plasmid sequence coverage > 80%, e-value < $1 \cdot e^{-23}$, and sequence identity > 98%. ARGs in plasmid, phage, proviruses, and phage-plasmid sequences were characterized using the same method and threshold as for the rMAGs. To identify potentially horizontal transfer events of ARGs via MGEs, we carefully examined the sequence identity of ARGs shared between rMAGs and MGEs using BLAST [32]. Those with > 99% identity, e-value ≤$1 \cdot e^{-5}$, and 100% coverage were considered to have been transferred horizontally.

Determination of phage–host interactions

Both *in situ* and *ex situ* hosts of the phages were identified integrally using four methods [28]: (i) host CRISPR spacers, (ii) integrated viral fragments in host genomes, (iii) host tRNA genes, and (iv) host *k*-mer signatures. CRISPR spacers in the rMAGs were identified using CRT (v.1.2) [39] and PILER-CR (v.1.0.6) [40]. The identified spacers were compared against vOTUs using parameters including BLASTn with ≤ 1 mismatch, 100% identity, and 100% coverage to establish virus–host links [41]. tRNA genes were independently identified in viral and host bacterial genomes using tRNAscan-SE 2.0 (v2.0.12) [42]. Subsequently, BLASTn (v2.14.0) was used to compare the predicted viral and bacterial tRNA sequences, retaining matches only if they exhibited 100% identity and 100% coverage [28]. Genomic regions shared between vOTUs and rMAGs were detected using BLASTn with thresholds of an identity ≥ 90%, a hit length ≥ 1000 bp, and e-value ≤ 0.001 [41]. The *k*-mer frequencies of sequences from rMAGs and vOTUs were estimated using WIsH (v.1.1) [43]. The host predicted by WIsH with the lowest P-value (≤ 10^{-5}) was retained for each vOTU [41]. Hosts predicted by any one of the four methods described above were retained for subsequent analyses of virus–host interactions. The network of virus–host links was visualized in Cytoscape (v.3.9.0) [44].

Phylogenetic and functional characterization of the novel genomes using comparative genomics

Eighty-two rMAGs reconstructed from this study were unclassified at the species level; therefore, they were considered novel. To facilitate the comparative genomic analysis, only high-quality novel genomes with completeness > 90% and contamination ≤ 5% that harbor high-risk ARGs were included and defined as key novel genomes. To infer the phylogeny of the key novel genomes, the reference genomes that fall within the taxonomic rank of the genus to which a specific novel genome belonged were downloaded from the GTDB database. A maximum-likelihood phylogenetic tree containing the key novel genomes and their corresponding reference genomes was constructed using FastTree (v2.1.11) [36]. Orthogroups (OGs) inference and gene duplication events were determined using OrthoFinder (v3.0.1b1) [44], based on all genomes included in the phylogenetic tree associated with each key novel genome. The potential functions of gene families in the key novel genomes were characterized using EggNOG-mapper (v2.1.12) [46]. Badirate (v1.35.0) [47] was used to infer the evolutionary history of gene families in each key novel genome, using its deepest-branch phylogenetic relatives as the reference. Given that none of the key novel genomes were complete, we focused only on the “expand” and “gain” events of the target genes. An "expand" event was defined as a scenario in which the gene in the key novel genome had shown a higher copy number than that in the reference, with an initial copy number greater than zero. In contrast, the “gain” events refer to the presence of the gene only in the novel genome but absent in the reference [48].

Results

Comprehensive profiling of microbial communities in the ICU setting

In this longitudinal study, five hospital surfaces and the on-duty nurses’ hands in an ICU ward were continuously monitored over six months (Fig. 1a). Following shotgun metagenomic sequencing and Kruskal-Wallis tests, alpha-diversity analysis revealed significant differences in Shannon diversity ($p = 2.33 \times 10^{-5}$), Pielou’s evenness ($p = 1.10 \times 10^{-4}$), and species richness ($p = 1.68 \times 10^{-4}$) across sampling sites. The microbial community on the inner surface of the ICU door exhibited the highest alpha diversity for all three metrics (Fig. 1b), likely due to minimal external disturbance from infrequent disinfection and limited direct skin contact compared to other high-touch surfaces. In contrast, the exterior of the respiratory mask displayed the lowest microbial diversity, likely because its surface receives microbial input predominantly from the patient’s own respiratory emissions, thereby limiting the source pool. Other high-touch surfaces, such as bed rails, nurse call buttons, and the computer mouse, exhibited comparable Shannon diversity indices, possibly due to similar levels of hand-mediated microbial transfer and disinfection practices.

The significant variations were also found in microbial community structure, as evidenced by the distinct clustering patterns of microbial communities grouped by sampling site (PERMANOVA test, $R^2 = 0.21$, pseudo-$F = 3.95$, $p < 0.01$) and sampling date ($R^2 = 0.27$, pseudo-$F = 3.06$, $p < 0.01$) (Fig. 1c). While PERMDISP indicated significant heterogeneity in within-group dispersion ($p < 0.01$ for both sampling site

and date), the distinct separation of clusters in the ordination plot, particularly for samples collected from the bed rail, left hand, inside of the ICU door, and the exterior of the respiratory mask, supported a genuine centroid shift in community composition among these sites. In contrast, samples collected from the nurse's right hand and high-touch surfaces (i.e., call button and computer mouse) showed substantial overlap, highlighting the homogeneity of microbial community profiles among these sampling types. This overlap may be attributed to the high frequency of contact by healthcare workers' dominant hand (i.e., the right hand), resulting in cross-transmission of microbes among these surfaces.

Site-specific microbial signatures and pathogen transmission patterns

Taxonomic profiling revealed a bacteria-dominated community (31.62 ± 14.97%) in clinical and skin surfaces, with smaller proportions of fungi (3.80 ± 5.20%) and viruses (0.14 ± 0.27%). Of the 11417 species identified, 6488 were shared across all sampling sites (**Fig. S2**). At each site, the relative abundance of dominant species such as *Malassezia restricta*, *Staphylococcus epidermidis*, and *Cutibacterium acnes* remained relatively stable over time (Fig. 2a). Within this stable background, we observed clear site-specific enrichments indicative of distinct transmission routes. Masks were uniquely enriched for cavity- and respiratory-tract-associated species, including *Moraxella osloensis*, *Streptococcus mitis*, *Streptococcus pneumoniae*, *Gemella haemolysans*, *Haemophilus parainfluenzae*, and *Rothia mucilaginosa*, suggesting a likely airborne or droplet-deposition pathway. Notably, several of these (e.g., *S. pneumoniae* and *S. mitis*) are opportunistic pathogens. In contrast, the nurses' hands showed significant enrichment of typical skin commensals (various *Corynebacterium* spp.) and the opportunistic pathogen *Pseudomonas aeruginosa*, suggesting a skin-resident signature distinct from that of inanimate surfaces. Crucially, key skin microbial commensals, such as *Corynebacterium tuberculostearicum* and *M. restricta*, were repeatedly identified on high-contact surfaces, including bed rails, nurse call buttons, computer mouse, and the ICU door, indicating potential persistent skin seeding on these clinical surfaces via contact transmission.

Among the detected microbial species, 319 were identified as pathogens (Fig. 2b), including 14 biosafety level 3 (BSL-3) and six ESKAPE pathogens (Fig. 2c). Although present at low relative abundances (< 0.1%), these high-risk taxa were consistently detectable in the ICU environment. To assess the role of contact in their spread, we modeled the dispersal of pathogens from the nurse's hand to surrounding ICU surfaces using Sloan's neutral community model (Fig. 2d). The model revealed a neutral dispersal pattern for the majority of BSL-3 and ESKAPE pathogens, indicating their dissemination was essentially stochastic, following the flow of skin contact **(Table S1)**. In contrast, a subset of pathogens, including the BSL-3 species *Pantoea agglomerans* and 20 BSL-2 species such as *Mycobacterium kansasii*, *Legionella pneumophila*, *Clostridium tetani*, and *Klebsiella aerogenes*, deviated significantly from neutral expectation (Fig. 2e). This pattern of active dissemination suggests these taxa may possess a stronger capacity to adapt to clinical surfaces. Collectively, these findings highlight the crucial role of healthcare personnel as passive vectors for the stochastic transmission of a wide range of pathogens and as

potential agents introducing specific, surface-adapted opportunistic pathogens into hospital environments through routine care activities.

Genome-level resistome profiling and growth rate estimation of pathogenic and novel genomes

Following genome reconstruction and dereplication, a total of 180 rMAGs were recovered from the ICU samples, comprising 89 and 91 that were of medium and high quality, respectively. Among these, 98 rMAGs were classified at the species level, among which 15 were identified as known pathogens **(Table S2)**. The remaining rMAGs (45.56%) were considered potential novel genomes, as they were uncharacterized at the species level (hereafter referred to as novel genomes) (Fig. 3a).

The functional traits of the rMAGs, particularly those of pathogenic species and novel taxa, were characterized. Genome-level resistome profiling revealed the presence of 188 ARGs, 30.9% of which conferred resistance to multiple classes of antimicrobial compounds, including drugs, biocides, and heavy metals **(**Fig. 3b**)**. Besides, nearly one-third of ARGs (32.4%) conferred resistance specifically to antibiotics, including 17 ARGs that were linked to multidrug resistance. The other 11.7% of ARGs were particularly resistant to biocidal agents, with 11 of them associated with resistance to multiple biocides. The remaining 25% of ARGs conferred resistance to heavy metals, primarily targeting copper, arsenic, and mercury.

The health risks associated with these ARGs were evaluated using four established criteria (i.e., human accessibility, mobility, pathogenicity, and clinical relevance [24]. This assessment identified 18 high-risk ARGs distributed across the microbial community, appearing in known pathogens, non-pathogenic microorganisms, and novel genomes (**Table S3 and** Fig. 4a). For example, the novel *Neisseria* genome (525_bin.20) and *Pseudomonas* genome (330_bin.15) harbored *macA* and *opmD* genes, respectively, encoding multidrug efflux pumps that confer resistance to various classes of antibiotics. Among other high-risk ARGs, *qacAB* encoding the major facilitator superfamily (MFS) pump, conferring resistance to biocides such as QACs and chlorhexidine [49]), was identified in *Staphylococcus hominis* (330_bin.11) and *Gemella sanguinis* (406_bin.8). Several ARGs encoding resistance-nodulation-division (RND) family pumps, including *crp*, *adeJ*, *sme*, *mexE*, *mexF*, *mexH*, and *oprN*, were frequently detected in both novel genomes (e.g., *Acinetobacter* (330_bin.7) and *Pseudomonas* (330_bin.15)), and the HAI-linked pathogen *Acinetobacter junii* (817_bin.50) [50]. Finally, four high-risk ARGs conferring beta-lactam resistance (*cfx*, *mecI*, *mecA*, and *oxa*) were localized within novel genomes such as *Prevotella* (406_bin.2) and *Porphyromonas_A* (817_bin.2), and the opportunistic pathogen *S. hominis* (330_bin.11) (**Table S3 and** Fig. 4a).

Because the incidence of HAI is driven by both pathogen abundance and metabolic activity, we investigated the enrichment dynamics and growth states (estimated via GRiD) of known pathogens and rMAGs carrying high-risk ARGs. Our analysis revealed that *Corynebacterium glucuronolyticum* associated with genitourinary tract infections, maintained relatively high abundance over time but exhibited generally low growth rates (mean GRiD < 1.5) (Fig. 3c). In contrast, several other highly abundant taxa

demonstrated more active growth states (GRiD ≥ 1.5), including pathogens such as skin commensal *Micrococcus luteus* (BSL-1), respiratory tract commensal *Rothia dentocariosa* (BSL-2), and various *Staphylococcus* species including *S. hominis* (330_bin.11) and *S. epidermidis* (413_bin.7 and 511_bin.6), which were classified as BSL-2 organisms. Notably, a novel *Stenotrophomonas* genome (330_bin.14) carrying *sme* gene encoding RND-family efflux pump maintained low abundance relative to dominant taxa, but displayed a consistently high growth rate (average GRiD = 3.22). Similarly, several novel genomes belonging to the genera of *Prevotella*, *Neisseria*, *Porphyromonas_A*, *Pseudomonas*, and *Pseudomonas_E*, exhibited active growth phases at multiple time points. These findings suggest that novel genomes harboring high-risk ARGs may be proliferating actively within the ICU environment despite their overall low abundance, posing a potential long-term health risk to immunocompromised patients.

MGE-mediated horizontal transfer of ARGs in clinical environments

To investigate potential ARG mobilization events, we reconstructed 1145 vOTUs, including 453 phages, and classified them using host-linkage evidence (*in situ* hosts). In addition, 178 plasmid sequences carrying ARGs were identified within the recovered rMAGs. Notably, one circular plasmid with direct terminal repeat (DTR) topology was identified in a HAI-linked pathogen *S. hominis* (330_bin.11). This plasmid harbored a *tetK* gene, which encoded an MFS efflux system conferring tetracycline resistance, and an MOBV-type relaxase (Fig. 4b). The presence of this relaxase facilitates the mobilization and transfer of the plasmid during conjugation, driving the dissemination of resistance genes within bacterial populations in clinical environments[51]. Although predominantly associated with the genus *Staphylococcus*, this plasmid was also detected in *Mammaliicoccus vitulinus*, *Sphingobacterium multivorum*, and the opportunistic pathogen *P. aeruginosa* (Fig. 4c). This broad cross-species distribution strongly suggests that HGT events contribute to the environmental persistence of this resistance element.

In addition to the circular plasmid, two additional plasmids lacking detectable terminal repeats were identified within a single phage sequence, defining them as a “phage-plasmid”, were recovered from *G. sanguinis* (406_bin.8, "Plasmid1") and the opportunist pathogen *S. hominis* (330_bin.11, "Plasmid2") (Fig. 4d). Notably, this phage-plasmidcontains a replicon assigned to the rep_cluster_2120 plasmid replication cluster, indicating its capability for stable replication and inheritance within the host. Furthermore, it exhibited high sequence similarity (Mash distance < 0.06) to the *pAQZ1* plasmid originally identified in *S. epidermidis*. Given that *pAQZ1* harbors multiple ARGs conferring resistance to diverse antimicrobial compounds [52], this high degree of similarity suggests that the identified phage–plasmid may also function as a mobile vector, facilitating the horizontal transmission of resistance genes across diverse species.

As a result, extensive HGT of ARGs mediated by a diverse range of MGEs, including plasmids, phages, prophages, and phage-plasmids, was observed (**Table S3 and** Fig. 4a). In particular, high-risk ARGs were

frequently mobilized into novel genomes and into known pathogens via plasmid-mediated transfer. For instance, the *mexF* and *mexE* genes were transferred through an identical plasmid into two phylogenetically related novel genomes, *Pseudomonas* (330_bin.15) and *Pseudomonas_E* (316_bin.6). Similarly, the genes *tetK* in *S. hominis* (330_bin.11) and *emrC* in *G. sanguinis* (406_bin.8) were acquired through plasmid-mediated HGT. In contrast, the *qacAB* and *qacR* genes were transferred between these two species by the same phage-plasmid. Beyond high-risk elements, HGT of low-risk ARGs was also prevalent. Examples include the transfer of the genes *triA, triB*, and *triC* by plasmids, and *parR* and *parS* by phage within the novel *Pseudomonas* (330_bin.15) genome. Furthermore, in two *Staphylococcus* species, *S. capitis* (511_bin.33) and *S. epidermidis* (406_bin.15), several metal-resistance genes, including *arsC* and *mgrA*, were acquired through phage-mediated HGT. Taken together, these observations suggest that clinical environments may facilitate ARG dissemination via HGT, potentially driven by intensive selective pressures such as antibiotic use and biocidal agents [53].

Comparative genomics revealed the potential adaptation strategies of key novel genomes in ICU environments

To explore the evolutionary history of key novel genomes that may have experienced within the harsh hospital environments, seven high-quality rMAGs harboring high-risk ARGs were selected for comparative genomic analysis using their phylogenetically closest relatives (genome similarity with an ANI value > 99%) that are known to cause human diseases as reference genomes (Fig. 5 **and Figs. S3-S5**). Given that these key novel genomes were not fully closed, our analysis focused primarily on OG functions characterized by "expansion" or "gain" events. Our results revealed increased copy number for genes associated with the metabolism and detoxification of biocides across several key novel genomes. For example, genes involved in the breakdown of common clinical biocides, including alcohols, alkylating agents, and phenolic compounds (*adh*, *adhp*, *nad*, *qor*, and *ylil*), showed copy number amplification in novel *Stenotrophomonas* and *Pseudomonas* genomes. Specifically, the expansion of the *katA* gene in a novel *Stenotrophomonas* (330_bin.14) genome may enhance resistance to potent oxidizing agents such as hydrogen peroxide (H_2O_2), a common hospital biocide (**Fig. S4**). In *Pseudomonas* (330_bin.15) and *Pseudomonas_E* (817_bin.24 and 316_bin.6), we observed expansion in genes (*gst*, *yfcG*, *gsiB, gsiC, gsiD*, and *gpx*) involved in oxidative stress mitigation and DNA repair (*umuD*, *vsr*, and *recN*). While the former set helps detoxify reactive oxygen species (ROS), the latter group facilitates the recognition and repair of ROS-induced DNA damage. Together, these metabolic adaptations may accelerate the degradation of biocides and mitigate oxidative stress, significantly enhancing bacterial survival in chemically hostile hospital environments.

Similar to the adaptation observed with biocides, genes conferring resistance to antibiotics and heavy metals also exhibited expansion across a wide range of genera (Fig. 5 **and Fig. S3-S5**). Notably, novel genomes belonging to the genera *Pseudomonas_E* (316_bin.6 and 817_bin.24) and *Neisseria* (525_bin.20) contained amplified genes encoding MFS transporters, particularly within the Drug:H+ Antiporter (DHA) families DHA1 (*mdfA*, *yitG*, *bcr*, *cmlA*, and *lmrB*) and DHA2 (*emrB*, *lmrB*, and *norB*). In addition, genes encoding two-component systems that modulate antibiotic resistance were notably

expanded. For example, in *Pseudomonas_E* (316_bin.6), we identified expansions in the EvgA/S system, which regulates multiple MDR efflux pumps, and the *PhoPQ* system, which mediates lipid A modifications associated with resistance to polymyxins and aminoglycosides [54]. Furthermore, genes encoding acetylation-related enzymes (*catA*, *catB*, and *vat*) were amplified across multiple genera, including *Pseudomonas, Acinetobacter*, and *Stenotrophomonas*. These enzymes can inactivate streptogramins and chloramphenicol by acetylating the target antibiotics [55]. Finally, several novel genomes exhibited expanded resistance potential to heavy metals. This included an increased copy number of genes conferring resistance to arsenic (*arsB*, *arsC*, *arsH*, *arsM*, and *arsR*) in *Pseudomonas_E*, *Stenotrophomonas*, and *Pseudomonas*, copper in *Pseudomonas_E* (*cueR* and *czcC*, 817_bin.24) and *Neisseria* (*czcD*, 525_bin.20), and nickel (*nikA* and *nikC*) and zinc (*zntR*) in a *Pseudomonas_E* (817_bin.24).

As an additional strategy to limit the penetration of biocides and antibiotics, biofilm-associated genes were amplified across several taxa, reinforcing physical barriers and improving environmental persistence. These expanded genes correspond to distinct, sequential stages of biofilm development. During the initial attachment stage, genes encoding core chemotaxis regulators (*cheA*, *cheB*, and *cheY*) were expanded, likely guiding bacterial movement toward favorable surfaces. This stage also involved the expansion of fimbrial adhesion proteins (*fimA, fimB, fimC, fimD, fimF, fimH, fimI, ecpD*, and *papD*) and Type IV pili components (*pilB, pilT, pilH, and pilU*), which collectively facilitate stable surface anchoring. During microcolony formation, expanded regulatory genes (*gacS, sinR, crp, relA, spot*) likely promote coordinated cell behavior and support early matrix development [56–58]. Simultaneously, key extracellular polysaccharide (EPS) biosynthesis genes exhibited amplification. Early-stage EPS genes (*gumF, gumG*, *pgaC*, and *icaA*) contribute to the initiation of matrix formation. In contrast, genes involved in mature EPS production and structural organization (*algK, wcaE, pslL, epsH, epsJ, pelF, cpsE*, and *amsB*) facilitate the development of a stable and protective biofilm architecture [59]. Collectively, these genetic expansions likely enhance the structural resilience of biofilms, increasing the tolerance of bacterial members to both chemical biocides and antimicrobial agents in the ICU.

Beyond antimicrobial resistance, several novel genomes exhibited expanded virulence features, further underscoring their pathogenic potential. In *Pseudomonas* rMAG (330_bin.15), we identified an expansion of *exoU*, which encodes a potent cytotoxin that induces pyroptotic cell death in host tissues, particularly during chronic infections. This rMAG also harbored an expanded *icmF* gene, which plays a critical role in coordinating toxin secretion with quorum sensing [56]. Together, these factors may enhance the bacterium's ability to modulate host immune responses and establish persistent infections. In *Pseudomonas_E* rMAG (817_bin.24), expansion was observed across multiple genes encoding essential components of the type IV secretion system (T4SS), including conjugative transfer proteins (*trb* gene families) and virulence effectors (*virB* gene families) (**Fig. S3**), which facilitate the dissemination of virulence traits via HGT [56]. Moreover, amplification of key T4SS-associated ATPases, such as *virD4* and *dotB*, suggests reinforcement of the secretion machinery’s coupling and energy-supplying modules [56]. Collectively, the amplification of these secretion systems and effector genes may lead to heightened toxin delivery and increased pathogenicity in clinical environments.

Discussion

Despite the routine application of intensive disinfection protocols designed to minimize the environmental biomass, hospital surfaces remain dynamic microbial reservoirs continuously reshaped by human input. Our findings indicate a profound level of microbial connectivity, with over 6,000 microbial species shared between healthcare workers' hands and hospital surfaces. Sloan's neutral model further quantified this exchange, predicting strong transmissibility for 856 species, including 25 established pathogens, from nurses' hands to inanimate hospital surfaces. This underscores the central role of healthcare workers as primary vectors mediating microbial dispersal via skin touch. Consequently, common skin commensals such as *S. epidermidis*, *C. acnes*, and *M. restricta* were consistently detected from hospital surfaces, likely originating from continuous skin shedding or direct contact [60]. Similarly, oropharyngeal and respiratory taxa, such as *M. osloensis* and *S. mitis*, likely colonize these surfaces through exhaled aerosols, as evidenced by their presence on the exterior of respiratory masks.

Following initial seeding from human reservoirs, the long-term metabolic status of microbes on inanimate hospital surfaces is determined by their ability to adapt to the stable yet restrictive environmental conditions of the ICU. Our six-month longitudinal study showed that the clinical environmental filters remain constant, favoring species capable of physiological vigor despite chronic nutrient scarcity and chemical stress. For many commensals, the transition from the human body to a clinical surface leads to a state of metabolic decline. A prominent example is *C. glucuronolyticum*, a commensal typically associated with the genitourinary tract [61] that consistently exhibits a low growth rate (GRiD < 1.5). While it is frequently reintroduced through human activity, its metabolism is highly specialized for the human host environment. The stable, lower ambient temperatures of the ICU (25°C compared to the host's 37°C) and the lack of host-specific substrates act as significant inhibitors, preventing this species from transitioning into an active growth state on inanimate hospital surfaces.

In contrast, several skin commensals with HAI-linked pathogenic potential, including *S. epidermidis* and *S. hominis*, maintained a relatively active growth state (mean GRiD > 1.5). Typically, these *Staphylococcus* species are fastidious, requiring specific lipids found in human sebum and sugars and trace elements in human sweat to support their growth [62]. However, their ability to maintain active replication despite the scarcity of these host-derived nutrients suggests a strong metabolic plasticity and active environmental defense. This active growth is likely enabled by a detoxification strategy that alleviates the metabolic stalling usually caused by biocide exposure, as evidenced by the presence of peroxide resistance (*perR*) and phenolic compound resistance (*fabI*) genes across these two *Staphylococcus* species. Furthermore, the acquisition of high-risk ARGs through MGE might also benefit bacterial growth. Specifically, the plasmid-mediated *tetK* gene and phage-plasmid-mediated *qacAB* gene encode the MFS efflux system. By actively extruding biocides, such as QACs, and antibiotics, such as tetracycline, these pumps keep the internal cellular environment clean, allowing staphylococcal metabolic machinery to continue replicating despite the hostile external conditions.

The ability to maintain active growth under stable selective pressure is also evident in ubiquitous specialists like *M. luteus*. Throughout the study, *M. luteus* maintained a relatively higher growth rate (mean GRiD > 1.79), likely supported by its ability to synthesize carotenoid pigments, which may help neutralize ROS generated by routine disinfection [63]. When coupled with its inherent desiccation tolerance and ability to utilize trace organic residues [64, 65], *M. luteus*, along with the aforementioned *Staphylococcus* species, effectively occupies the ecological niches left vacant by less resilient commensals. Collectively, these findings suggest that the ICU environment does not merely serve as a passive transit point, but may instead facilitate the establishment of a specialized "resident" community that employs active detoxification and scavenging to achieve long-term environmental persistence.

In response to ongoing stress from disinfectant practices, certain bacterial pathogens may have evolved specialized genomic toolkits to colonize clinical environments. For example, a novel *Stenotrophomonas* species, which is closely related to the opportunistic nosocomial pathogen *S. maltophilia* [60–62], exhibited low relative abundance over time; however, it displayed a consistently high growth rate (GRiD = 3.2). This metabolic vigor is likely sustained by the Sme RND-family efflux pump, which actively extrudes toxic biocides and antibiotics before they can inhibit cellular function [66]. Furthermore, the amplification of genes associated with the metabolism of hydrogen peroxide, alcohol, alkylating agents, and phenolic compounds, the common active ingredients in hospital biocides, suggests this novel taxon does not merely survive but may actively use or detoxify these chemical stressors. Similarly, the novel *Pseudomonas* species (ANI > 99% to *P. aeruginosa*, an ESKAPE pathogen) exhibited a distinct adaptation strategy. While their growth rate was relatively slow, their genomes were significantly enriched in genes dedicated to detoxifying ROS and repairing ROS-induced DNA damage. This suggests a strategy of high-fidelity maintenance rather than rapid proliferation. By using efflux systems from the ABC, MFS, and MDR families with broad substrate specificity, these novel taxa enhance their tolerance to the complex, fluctuating chemical landscape of the ICU, including biocides, heavy metals, and multi-class antibiotics.

The persistence of these microbes is not merely an individual effort; instead, they form organized consortia to resist environmental pressure. We observed a significant enrichment of biofilm-associated genes and those involved in the secretion of extracellular polymeric substances (EPS) within these key novel genomes. These structures serve as both physical and chemical barriers, sheltering the community from antimicrobial penetration agents. Beyond physical protection, the close spatial proximity within these biofilms facilitates the HGT of resistance traits. Consistent with this, we identified evidence of MGE-mediated transfer across diverse taxa. For example, the *mexE* and *mexF* multidrug efflux genes were detected on identical plasmids within two novel *Pseudomonas* species. Similarly, the biocide resistance genes *qacAB* and *qacR* were transferred between *S. hominis* and *G. sanguinis* via a shared phage–plasmid element. While HGT-driven resistance sharing stabilizes the microbial community against routine disinfection, the resulting enrichment of ARGs inherently elevates the clinical risk. This threat is further escalated when such resistance traits are coupled with the amplification of virulence factors. Notably, in one novel *Pseudomonas_E* species, we observed the co-occurrence of high-risk ARGs and an amplification of secretion systems and exotoxin effectors. This convergence of multidrug

resistance and enhanced pathogenic potentials in novel ICU-resident taxa underscores the need for genome surveillance of inanimate hospital surfaces.

Collectively, our results indicate that, despite prolonged and intensive disinfection, hospital environmental surfaces persist as reservoirs of diverse microorganisms, including opportunistic pathogens encoding resistance to both biocidal agents and antimicrobial drugs. Several novel taxa, closely resembling known nosocomial pathogens, appear to possess genomic signatures suggesting specialized evolution in clinical environments, potentially enhancing their capacity to tolerate multiple antimicrobial stressors. This resilience is likely reinforced by a “consortium strategy” involving biofilm formation and the HGT-mediated dissemination of high-risk ARGs. Notably, the presence of these ARGs implies cross-resistance that may be driven by co-selection, specifically, chronic exposure to non-antibiotic stressors, such as biocides or other chemicals, may select for phenotypes that are simultaneously resistant to clinically relevant antibiotics [67]. Through such co-selection, resistant populations may persist and proliferate even in the absence of direct antibiotic exposure, ultimately increasing the therapeutic challenges should these environmental reservoirs transition to infecting vulnerable hosts. By integrating ecological and evolutionary perspectives, our findings provide a framework for evaluating the potential unintended consequences of clinical disinfection practices and highlight the value of incorporating evolutionary principles into infection control and antimicrobial stewardship. Such strategies are essential to ensure that hygiene protocols do not inadvertently facilitate the emergence of more resilient healthcare-associated pathogens.

Several limitations should be acknowledged in this study. First, the lack of microbial isolation and laboratory culture precluded experimental validation of predicted resistance phenotypes and pathogenic potential; therefore, the high growth rates and metabolic activities inferred through GRiD analysis remain computational predictions. Second, detailed information on specific ICU disinfection protocols and longitudinal patient clinical metadata was unavailable, limiting our ability to directly correlate resistance dynamics with specific clinical interventions. Future research integrating standardized disinfection records, patient-derived isolates, and experimental evolution studies under hospital-relevant chemical pressures will be critical to definitively elucidate the molecular trajectories by which antimicrobial stress shapes microbial genome evolution in clinical environments.

Declarations

Ethics approval and consent to participate

Ethics approval for subject sampling and publication of data originating from subjects included in this study was granted by the Xi’an Jiaotong-Liverpool University Ethics Committee (reference no. ER-LRR-110000816202311211022225).

Consent for publication

Not applicable.

Competing interests

The authors declare no competing interests.

Funding

This research was supported by the National Natural Science Foundation of China (82502773), Basic Research Program of Jiangsu (BK20230230), Research Development Fund (RDF-23-01-030), and Postgraduate Research Scholarship of Xi'an Jiaotong-Liverpool University (PGRS2306039) to X.T.

Author Contribution

S.Q. performed bioinformatic analysis, data analysis, and interpretation, and wrote the manuscript. L.H. performed sampling and metadata collection. L.S. performed total DNA extraction. S.C. performed bioinformatic analysis. X.H. and Q.Z. provided guidance in the study design and manuscript revision. Q.Z. supervised the sampling and metadata collection. X.T. conceived the study, supervised the research, and wrote the manuscript.

Acknowledgement

We thank Shicong Du and Danli Luo for their suggestions on data analysis. We also thank 3D Medicines for their assistance in library preparation and sequencing for the low-biomass ICU samples.

Data Availability

Raw DNA sequencing data for the ICU surface and human skin samples are available in the NCBI Sequence Read Archive (SRA) under the BioProject accession number PRJNA1298590. Metadata and in-house scripts used for data analysis are available on GitHub at https://github.com/Shijiao7/SZ_ICU_microbiota.

References

1. Tozzo P, Delicati A, Caenazzo L. Human microbiome and microbiota identification for preventing and controlling healthcare-associated infections: A systematic review. Front Public Health. 2022;10:989496. https://doi.org/10.3389/fpubh.2022.989496
2. Blot S, Ruppé E, Harbarth S, Asehnoune K, Poulakou G, Luyt C-E, et al. Healthcare-associated infections in adult intensive care unit patients: Changes in epidemiology, diagnosis, prevention and contributions of new technologies. Intensive Crit Care Nurs. 2022;70:103227. https://doi.org/10.1016/j.iccn.2022.103227

3. Chng KR, Li C, Bertrand D, Ng AHQ, Kwah JS, Low HM, et al. Cartography of opportunistic pathogens and antibiotic resistance genes in a tertiary hospital environment. Nat Med. 2020;26:941–51. https://doi.org/10.1038/s41591-020-0894-4
4. D'Souza AW, Potter RF, Wallace M, Shupe A, Patel S, Sun X, et al. Spatiotemporal dynamics of multidrug resistant bacteria on intensive care unit surfaces. Nat Commun. 2019;10:4569. https://doi.org/10.1038/s41467-019-12563-1
5. Maillard J-Y, Pascoe M. Disinfectants and antiseptics: mechanisms of action and resistance. Nat Rev Microbiol. 2024;22:4–17. https://doi.org/10.1038/s41579-023-00958-3
6. Fernández L, Hancock REW. Adaptive and mutational resistance: role of porins and efflux pumps in drug resistance. Clin Microbiol Rev. 2012;25:661–81. https://doi.org/10.1128/CMR.00043-12
7. Merchel Piovesan Pereira B, Wang X, Tagkopoulos I. Biocide-induced emergence of antibiotic resistance in *Escherichia coli*. Front Microbiol. 2021;12:640923. https://doi.org/10.3389/fmicb.2021.640923
8. Jin M, Liu L, Wang D, Yang D, Liu W, Yin J, et al. Chlorine disinfection promotes the exchange of antibiotic resistance genes across bacterial genera by natural transformation. ISME J. 2020;14:1847–56. https://doi.org/10.1038/s41396-020-0656-9
9. Michaelis C, Grohmann E. Horizontal gene transfer of antibiotic resistance genes in biofilms. Antibiotics. 2023;12:328. https://doi.org/10.3390/antibiotics12020328
10. Schubert M, Lindgreen S, Orlando L. AdapterRemoval v2: rapid adapter trimming, identification, and read merging. BMC Res Notes. 2016;9:88. https://doi.org/10.1186/s13104-016-1900-2
11. Li D, Luo R, Liu C-M, Leung C-M, Ting H-F, Sadakane K, et al. MEGAHIT v1.0: a fast and scalable metagenome assembler driven by advanced methodologies and community practices. Methods. 2016;102:3–11. https://doi.org/10.1016/j.ymeth.2016.02.020
12. Wood DE, Lu J, Langmead B. Improved metagenomic analysis with Kraken 2. Genome Biol. 2019;20:257. https://doi.org/10.1186/s13059-019-1891-0
13. Lu J, Breitwieser FP, Thielen P, Salzberg SL. Bracken: estimating species abundance in metagenomics data. PeerJ Comput Sc*i*. 2017;3:e104. https://doi.org/10.7717/peerj-cs.104
14. Guo C, Chen Q, Fan G, Sun Y, Nie J, Shen Z, et al. gcPathogen: a comprehensive genomic resource of human pathogens for public health. Nucleic Acids Res. 2024;52:D714–23. https://doi.org/10.1093/nar/gkad875
15. Sloan WT, Lunn M, Woodcock S, Head IM, Nee S, Curtis TP. Quantifying the roles of immigration and chance in shaping prokaryote community structure. Environ Microbiol. John Wiley & Sons, Ltd; 2006;8:732–40. https://doi.org/10.1111/j.1462-2920.2005.00956.x
16. Uritskiy GV, DiRuggiero J, Taylor J. MetaWRAP, a flexible pipeline for genome-resolved metagenomic data analysis. Microbiome. 2018;6:158. https://doi.org/10.1186/s40168-018-0541-1
17. Olm MR, Brown CT, Brooks B, Banfield JF. dRep: a tool for fast and accurate genomic comparisons that enables improved genome recovery from metagenomes through de-replication. ISME J. 2017;11:2864–8. https://doi.org/10.1038/ismej.2017.126

18. Von Meijenfeldt FAB, Arkhipova K, Cambuy DD, Coutinho FH, Dutilh BE. Robust taxonomic classification of uncharted microbial sequences and bins with CAT and BAT. Genome Biol. 2019;20:217. https://doi.org/10.1186/s13059-019-1817-x
19. Parks DH, Chuvochina M, Rinke C, Mussig AJ, Chaumeil P-A, Hugenholtz P. GTDB: an ongoing census of bacterial and archaeal diversity through a phylogenetically consistent, rank normalized and complete genome-based taxonomy. Nucleic Acids Res. 2022;50:D785–94. https://doi.org/10.1093/nar/gkab776
20. Aroney STN, Newell RJP, Nissen JN, Camargo AP, Tyson GW, Woodcroft BJ. CoverM: read alignment statistics for metagenomics. Bioinformatics. 2025;41:btaf147. https://doi.org/10.1093/bioinformatics/btaf147
21. Emiola A, Oh J. High throughput in situ metagenomic measurement of bacterial replication at ultra-low sequencing coverage. Nat Commun. 2018;9:4956. https://doi.org/10.1038/s41467-018-07240-8
22. Doster E, Lakin SM, Dean CJ, Wolfe C, Young JG, Boucher C, et al. MEGARes 2.0: a database for classification of antimicrobial drug, biocide and metal resistance determinants in metagenomic sequence data. Nucleic Acids Res. 2020;48:D561–9. https://doi.org/10.1093/nar/gkz1010
23. Du S, Lin H, Luo Q, Man CL, Lai SH, Ho KF, et al. House dust microbiome differentiation and phage-mediated antibiotic resistance and virulence dissemination in the presence of endocrine-disrupting chemicals and pharmaceuticals. Microbiome. 2025;13:96. https://doi.org/10.1186/s40168-025-02081-2
24. Zhang Z, Zhang Q, Wang T, Xu N, Lu T, Hong W, et al. Assessment of global health risk of antibiotic resistance genes. Nat Commun. 2022;13:1553. https://doi.org/10.1038/s41467-022-29283-8
25. Nissen JN, Johansen J, Allesøe RL, Sønderby CK, Armenteros JJA, Grønbech CH, et al. Improved metagenome binning and assembly using deep variational autoencoders. Nat Biotechnol. 2021;39:555–60. https://doi.org/10.1038/s41587-020-00777-4
26. Johansen J, Plichta DR, Nissen JN, Jespersen ML, Shah SA, Deng L, et al. Genome binning of viral entities from bulk metagenomics data. Nat Commun. 2022;13:965. https://doi.org/10.1038/s41467-022-28581-5
27. Nayfach S, Camargo AP, Schulz F, Eloe-Fadrosh E, Roux S, Kyrpides NC. CheckV assesses the quality and completeness of metagenome-assembled viral genomes. Nat Biotechnol. 2021;39:578–85. https://doi.org/10.1038/s41587-020-00774-7
28. Du S, Tong X, Lai ACK, Chan CK, Mason CE, Lee PKH. Highly host-linked viromes in the built environment possess habitat-dependent diversity and functions for potential virus-host coevolution. Nat Commun. 2023;14:2676. https://doi.org/10.1038/s41467-023-38400-0
29. Arndt D, Grant JR, Marcu A, Sajed T, Pon A, Liang Y, et al. PHASTER: a better, faster version of the PHAST phage search tool. Nucleic Acids Res. 2016;44:W16–21. https://doi.org/10.1093/nar/gkw387
30. Hyatt D, Chen G-L, LoCascio PF, Land ML, Larimer FW, Hauser LJ. Prodigal: prokaryotic gene recognition and translation initiation site identification. BMC Bioinformatics. 2010;11:119.

https://doi.org/10.1186/1471-2105-11-119

31. Camargo AP, Roux S, Schulz F, Babinski M, Xu Y, Hu B, et al. Identification of mobile genetic elements with geNomad. Nat Biotechnol. 2024;42:1303–12. https://doi.org/10.1038/s41587-023-01953-y
32. Wang X, Zhang H, Yu S, Li D, Gillings MR, Ren H, et al. Inter-plasmid transfer of antibiotic resistance genes accelerates antibiotic resistance in bacterial pathogens. ISME J. 2024;18:wrad032. https://doi.org/10.1093/ismejo/wrad032
33. Robertson J, Nash JHE. MOB-suite: software tools for clustering, reconstruction and typing of plasmids from draft assemblies. Microb Genom. 2018;4. https://doi.org/10.1099/mgen.0.000206
34. Katoh K, Standley DM. MAFFT multiple sequence alignment software version 7: improvements in performance and usability. Mol Biol Evol. 2013;30:772–80. https://doi.org/10.1093/molbev/mst010
35. Capella-Gutiérrez S, Silla-Martínez JM, Gabaldón T. trimAl: a tool for automated alignment trimming in large-scale phylogenetic analyses. Bioinformatics. 2009;25:1972–3. https://doi.org/10.1093/bioinformatics/btp348
36. Price MN, Dehal PS, Arkin AP. FastTree: computing large minimum evolution trees with profiles instead of a distance matrix. Mol Biol Evol. 2009;26:1641–50. https://doi.org/10.1093/molbev/msp077
37. Letunic I, Bork P. Interactive Tree Of Life (iTOL) v5: an online tool for phylogenetic tree display and annotation. Nucleic Acids Res. 2021;49:W293–6. https://doi.org/10.1093/nar/gkab301
38. Pfeifer E, Rocha EPC. Phage-plasmids promote recombination and emergence of phages and plasmids. Nat Commun. 2024;15:1545. https://doi.org/10.1038/s41467-024-45757-3
39. Bland C, Ramsey TL, Sabree F, Lowe M, Brown K, Kyrpides NC, et al. CRISPR Recognition Tool (CRT): a tool for automatic detection of clustered regularly interspaced palindromic repeats. BMC Bioinformatics. 2007;8:209. https://doi.org/10.1186/1471-2105-8-209
40. Edgar RC. PILER-CR: fast and accurate identification of CRISPR repeats. BMC Bioinformatics. 2007;8:18. https://doi.org/10.1186/1471-2105-8-18
41. Du S, Tong X, Leung MHY, Betts RJ, Woo AC, Bastien P, et al. Chronic exposure to polycyclic aromatic hydrocarbons alters skin virome composition and virus–host interactions. ISME J. 2024;18:wrae218. https://doi.org/10.1093/ismejo/wrae218
42. Chan PP, Lin BY, Mak AJ, Lowe TM. tRNAscan-SE 2.0: improved detection and functional classification of transfer RNA genes. Nucleic Acids Res. 2021;49:9077–96. https://doi.org/10.1093/nar/gkab688
43. Galiez C, Siebert M, Enault F, Vincent J, Söding J. WIsH: who is the host? Predicting prokaryotic hosts from metagenomic phage contigs. Bioinformatics. 2017;33:3113–4. https://doi.org/10.1093/bioinformatics/btx383
44. Otasek D, Morris JH, Bouças J, Pico AR, Demchak B. Cytoscape automation: empowering workflow-based network analysis. Genome Biol. 2019;20:185. https://doi.org/10.1186/s13059-019-1758-4

45. Emms DM, Kelly S. OrthoFinder: phylogenetic orthology inference for comparative genomics. Genome Biol. 2019;20:238. https://doi.org/10.1186/s13059-019-1832-y
46. Cantalapiedra CP, Hernández-Plaza A, Letunic I, Bork P, Huerta-Cepas J. eggNOG-mapper v2: functional annotation, orthology assignments, and domain prediction at the metagenomic scale. Mol Biol Evol. 2021;38:5825–9. https://doi.org/10.1093/molbev/msab293
47. Librado P, Vieira FG, Rozas J. BadiRate: estimating family turnover rates by likelihood-based methods. Bioinformatics. 2012;28:279–81. https://doi.org/10.1093/bioinformatics/btr623
48. Tong X, Luo D, Leung MHY, Lee JYY, Shen Z, Jiang W, et al. Diverse and specialized metabolic capabilities of microbes in oligotrophic built environments. Microbiome. 2024;12:198. https://doi.org/10.1186/s40168-024-01926-6
49. Abbood HM, Hijazi K, Gould IM. Chlorhexidine resistance or cross-resistance, that is the question. Antibiotics. 2023;12:798. https://doi.org/10.3390/antibiotics12050798
50. Kappstein I, Grundmann H, Hauer T, Niemeyer C. Aerators as a reservoir of *Acinetobacter junii*: an outbreak of bacteraemia in paediatric oncology patients. J Hosp Infect. 2000;44:27–30. https://doi.org/10.1053/jhin.1999.0648
51. Garcillán-Barcia MP, Francia MV, De La Cruz F. The diversity of conjugative relaxases and its application in plasmid classification. FEMS Microbiol Rev. 2009;33:657–87. https://doi.org/10.1111/j.1574-6976.2009.00168.x
52. Addetia A, Greninger AL, Adler A, Yuan S, Makhsous N, Qin X, et al. A novel, widespread *qacA* allele results in reduced chlorhexidine susceptibility in *Staphylococcus epidermidis*. Antimicrob Agents Chemother. 2019;63:e02607-18. https://doi.org/10.1128/AAC.02607-18
53. Lerminiaux NA, Cameron ADS. Horizontal transfer of antibiotic resistance genes in clinical environments. Can J Microbiol. 2019;65:34–44. https://doi.org/10.1139/cjm-2018-0275
54. Tierney AR, Rather PN. Roles of two-component regulatory systems in antibiotic resistance. Future Microbiol. 2019;14:533–52. https://doi.org/10.2217/fmb-2019-0002
55. Schwarz S, Shen J, Kadlec K, Wang Y, Brenner Michael G, Feßler AT, et al. Lincosamides, streptogramins, phenicols, and pleuromutilins: mode of action and mechanisms of resistance. Cold Spring Harb Perspect Med. 2016;6:a027037. https://doi.org/10.1101/cshperspect.a027037
56. Qin S, Xiao W, Zhou C, Pu Q, Deng X, Lan L, et al. *Pseudomonas aeruginosa*: pathogenesis, virulence factors, antibiotic resistance, interaction with host, technology advances and emerging therapeutics. Signal Transduct Target Ther. 2022;7:199. https://doi.org/10.1038/s41392-022-01056-1
57. Xu X, Li H, Qi X, Chen Y, Qin Y, Zheng J, et al. *cheA*, *cheB*, *cheR*, *cheV*, and *cheY* are involved in regulating the adhesion of *Vibrio harveyi*. Front Cell Infect Microbiol. 2021;10:591751. https://doi.org/10.3389/fcimb.2020.591751
58. Yin W-L, Xie Z-Y, Zeng Y-H, Zhang J, Long H, Ren W, et al. Two (p)ppGpp synthetase genes, *relA* and *spoT*, are involved in regulating cell motility, exopolysaccharides production, and biofilm formation of *Vibrio alginolyticus*. Front Microbiol. 2022;13:858559. https://doi.org/10.3389/fmicb.2022.858559

59. Kaplan JB, Velliyagounder K, Ragunath C, Rohde H, Mack D, Knobloch JK-M, et al. Genes involved in the synthesis and degradation of matrix polysaccharide in *Actinobacillus actinomycetemcomitans* and *Actinobacillus pleuropneumoniae* biofilms. J Bacteriol. 2004;186:8213–20. https://doi.org/10.1128/JB.186.24.8213-8220.2004
60. Lax S, Sangwan N, Smith D, Larsen P, Handley KM, Richardson M, et al. Bacterial colonization and succession in a newly opened hospital. Sci Transl Med. 2017;9:eaah6500. https://doi.org/10.1126/scitranslmed.aah6500
61. Meštrović T, Wilson J, Ljubin-Sternak S, Sviben M, Bedenić B, Barać A, et al. A 'pathogenic needle' in a 'commensal haystack': genetic virulence signatures of *Corynebacterium glucuronolyticum* that may drive its infectious propensity for the male urogenital system. Med Hypotheses. 2019;126:38–41. https://doi.org/10.1016/j.mehy.2019.03.011
62. Swaney MH, Nelsen A, Sandstrom S, Kalan LR. Sweat and sebum preferences of the human skin microbiota. Claesen J, editor. Microbiol Spectr. 2023;11:e04180-22. https://doi.org/10.1128/spectrum.04180-22
63. Chang Y-C, Lee P-H, Hsu C-L, Wang W-D, Chang Y-L, Chuang H. Decoding the impact of a bacterial strain of *Micrococcus luteus* on *Arabidopsis* growth and stress tolerance. Microorganisms. 2024;12:2283. https://doi.org/10.3390/microorganisms12112283
64. Nóbrega F, Duarte RTD, Torres-Ballesteros AM, Queiroz LL, Whyte LG, Pellizari VH. Cold adapted desiccation-tolerant bacteria isolated from polar soils presenting high resistance to anhydrobiosis. bioRxiv; 2021. https://doi.org/10.1101/2021.02.06.430066
65. Chaibenjawong P, Foster SJ. Desiccation tolerance in *Staphylococcus aureus*. Arch Microbiol. 2011;193:125–35. https://doi.org/10.1007/s00203-010-0653-x
66. Brooke JS. Advances in the microbiology of *Stenotrophomonas maltophilia*. Clin Microbiol Rev. 2021;34:e00030-19. https://doi.org/10.1128/CMR.00030-19
67. Virieux-Petit M, Hammer-Dedet F, Aujoulat F, Jumas-Bilak E, Romano-Bertrand S. From copper tolerance to resistance in *Pseudomonas aeruginosa* towards patho-adaptation and hospital success. Genes. 2022;13:301. https://doi.org/10.3390/genes13020301

Figures

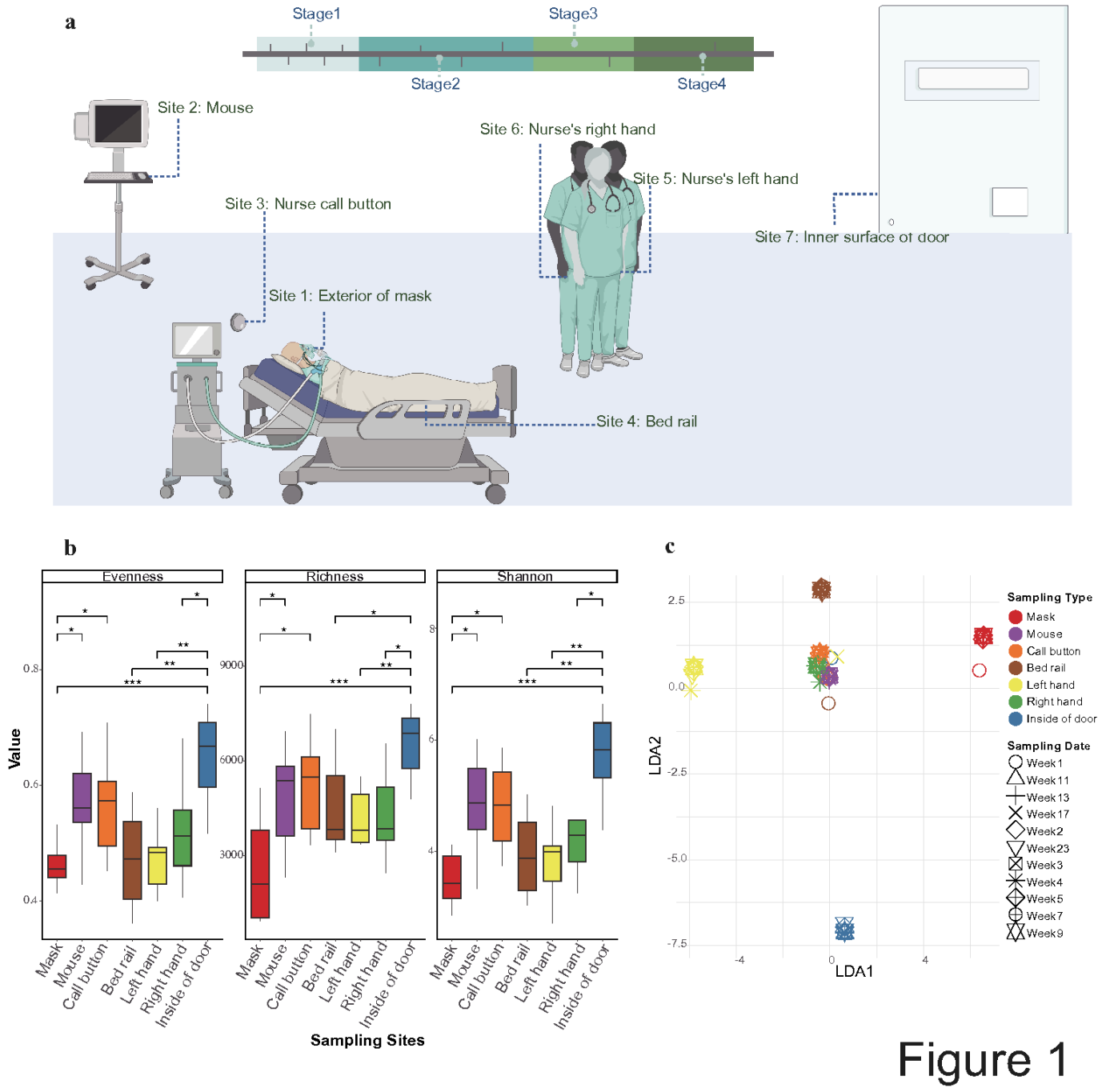


Figure 1

Figure 1

Longitudinal sampling scheme and the microbial community diversity in an intensive care unit (ICU). a) Overview of the six-month sampling scheme. Sampling was conducted across four distinct stages at five fixed environmental sites and two biological sites within a single ICU ward. Sites include: the external surface of the patient's respiratory mask on a fixed bed, the bedside computer mouse, the patient call bell, the bed handrails, the inner surface of the ICU door, and the nurse's left and right hands during each sampling event.**b) Alpha diversity of microbial communities**. Diversity indices are compared across the seven distinct sampling categories. Statistical significance is indicated by adjusted p-values

(p.adj < 0.001:"***", p.adj < 0.01:"**", p.adj < 0.05: "*"). **c) Beta-diversity of microbial community composition.** Ordination is based on Linear discriminant analysis (LDA) to illustrate the shifts and clustering in microbial community structure across sampling sites and weeks.

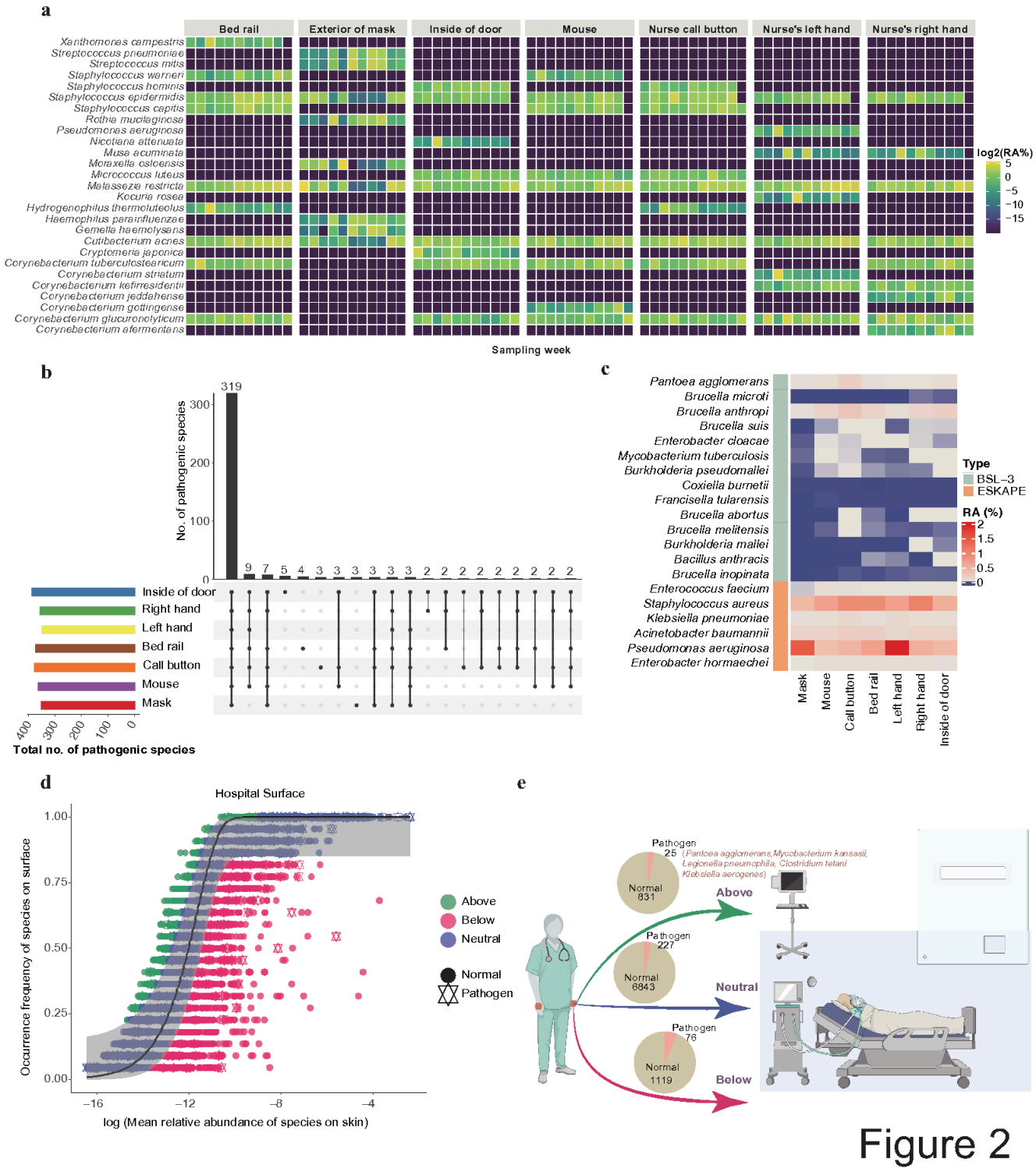


Figure 2

Figure 2

Colonization dynamics of dominant microbial species and skin-surface transmission potential within the ICU. a) Temporal dynamics of dominant microbial taxa. Heatmap displaying the relative abundance (RA) of the top 10 most abundant species across seven sampling sites. **b) Shared and site-specific pathogen distribution. c) Abundance of high-priority pathogens.**Mean relative abundance of Biosafety level 3 (BSL-3) and ESKAPE pathogens (including *Enterococcus faecium*, *Staphylococcus aureus*, *Klebsiella pneumoniae*, *Acinetobacter baumannii*, *Pseudomonas aeruginosa*, and *Enterobacter* species) across sampling sites and weeks. **d) Neutral model analysis of skin-to-surface microbial transmission.** Potential transmission from nurses' hands to hospital surfaces as predicted by Sloan's neutral model. Species are categorized into three partitions: "above-neutral" (indicating strong transmission potential), "neutral" (representing random dispersal), and "below-neutral" (indicating limited transmission potential). Hexagonal nodes represent pathogens, while circular nodes denote non-pathogenic bacteria. **e) Classification of pathogens across three partitions.** Percentage of pathogenic versus non-pathogenic species within each neutral model partition. Representative pathogens identified in the "above-neutral" and "neutral" partition groups are highlighted. Notably, BSL-3 pathogen *Pantoea agglomerans* in the "above-neutral" partition are classified as agents, while all remaining pathogens are classified as BSL-2; BSL-1 species are not listed.

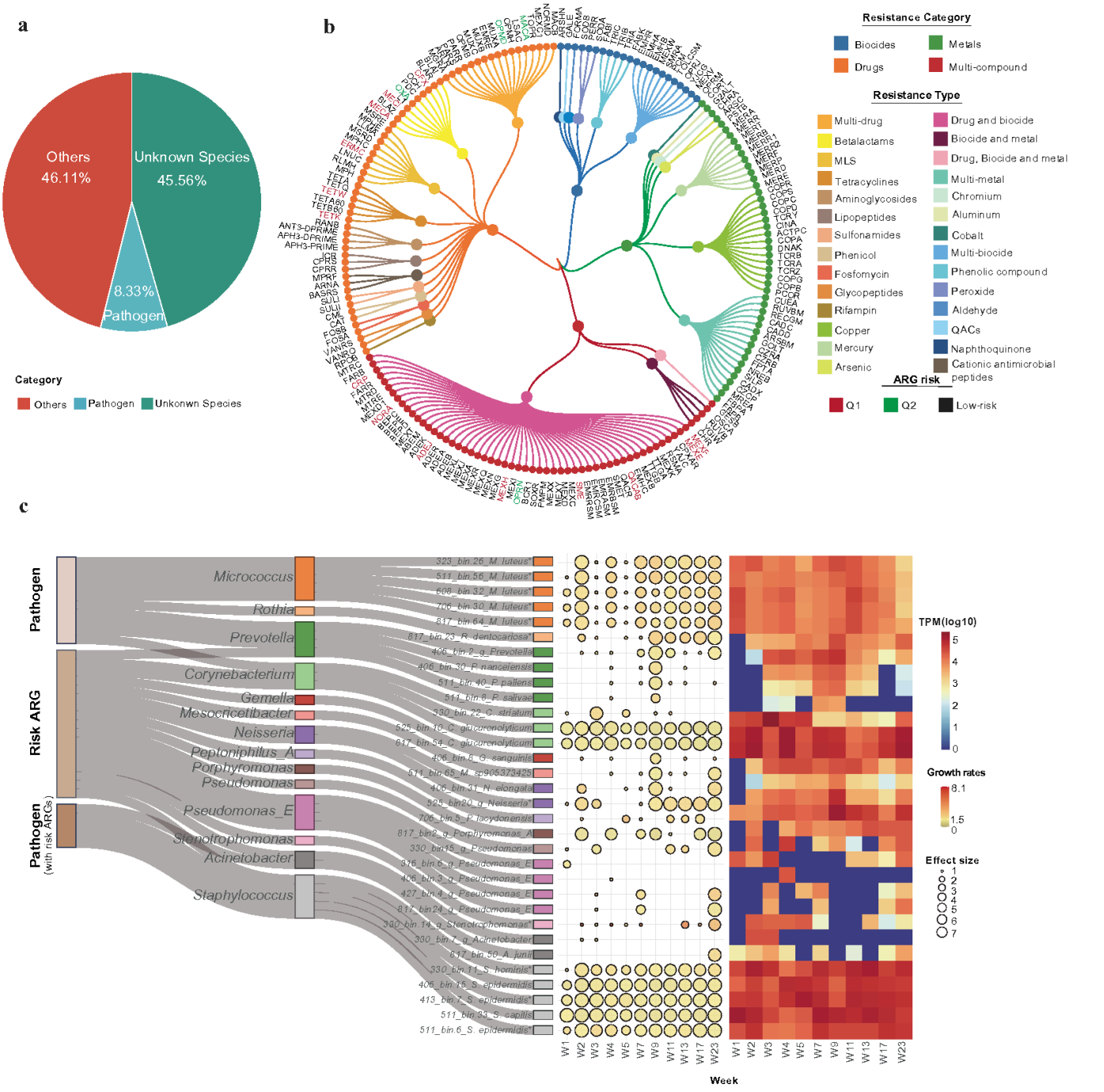


Figure 3

Figure 3

Taxonomic landscape, resistance profiles, and longitudinal dynamics of representative metagenome-assembled genomes (rMAGs). a) Taxonomic classification of rMAGs. Genomes are categorized into three groups: “Pathogen” (assigned to known pathogenic species), "Unknown species" (annotated at the genus or higher taxonomic ranks without a specific species assignment), and “Others” (rMAGs annotated as non-pathogens). **b) Profiles of antimicrobial resistance genes (ARGs) and resistance mechanisms.** ARGs are categorized by clinical risk; Q1 and Q2 are high-risk, while Q3 and Q4 are low-

risk. **c) Spatiotemporal growth and abundance dynamics.** The left panel highlights key rMAGs identified as potential pathogens (ranked at BSL-1 or above) or novel genomes harboring high-risk ARGs. In the central bubble plot, color intensity indicates the average predicted growth rate (GRiD), with GRiD >1.5 indicating active growth. Key rMAGs marked with an asterisk (*) represent taxa whose mean GRiD, calculated across all sampling dates, exceeded 1.5 and were therefore considered actively growing. Bubble size indicates the effect size, proportional to rMAG prevalence across all sampling sites for a given week. The right panel displays the corresponding relative abundances, normalized to transcripts per million (TPM).

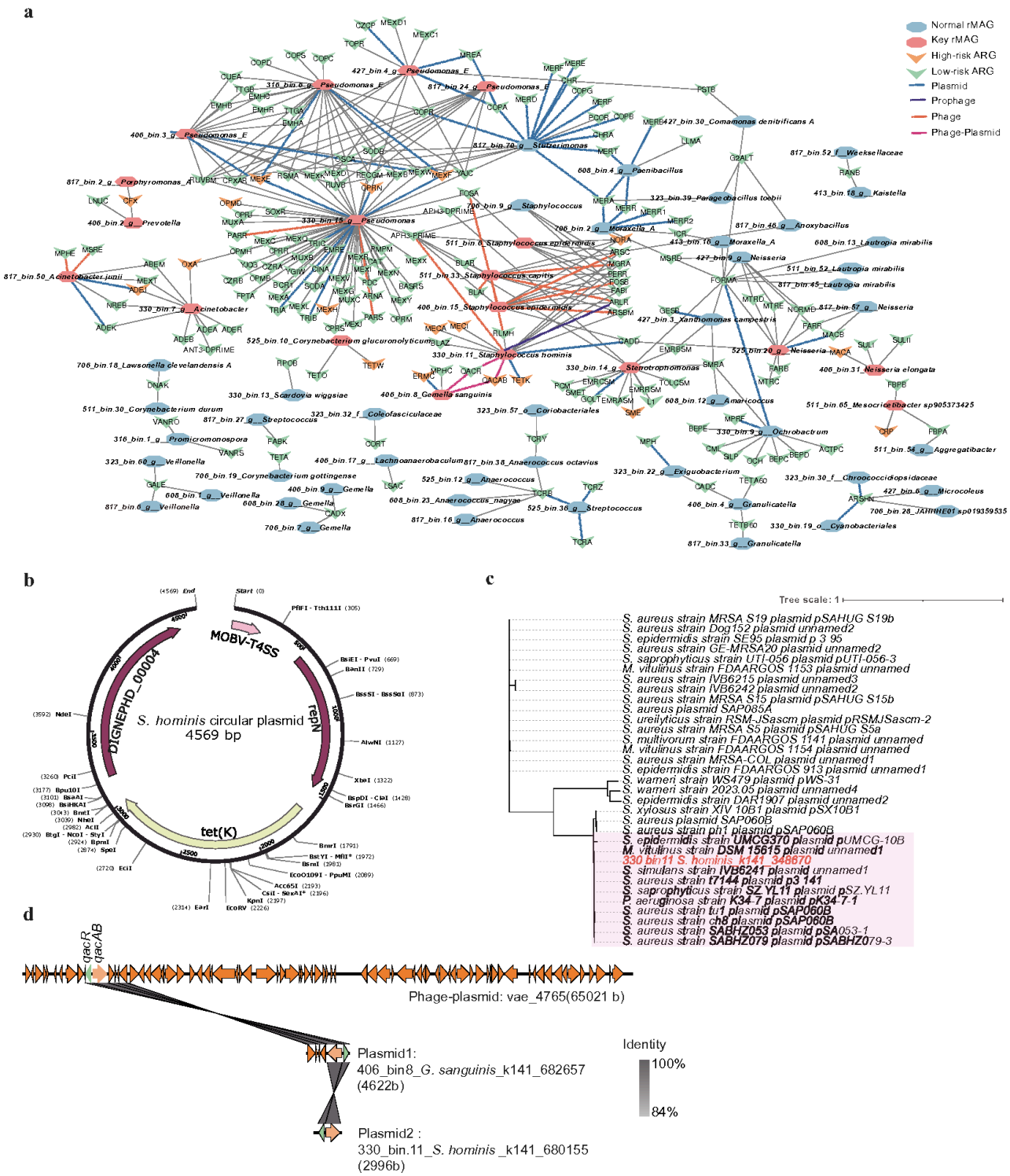


Figure 4

Figure 4

Horizontal gene transfer (HGT) of antimicrobial resistance genes (ARGs) among key rMAGs. a) HGT-mediated dissemination of high-risk ARGs. The heatmap illustrates the distribution of high-risk (Q1/Q2) ARGs within key rMAGs, including known pathogens or species-level unclassified genomes. The HGT events are mediated by four distinct types of mobile genetic elements (MGEs): plasmids, phages, prophages, and phage-plasmids. **b) A circular plasmid identified in *Staphylococcus hominis*.** Schematic

representation of a circular plasmid reconstructed from *S. hominis* (330_bin.11), a BSL-2 opportunistic pathogen. **c) Comparative genomic analysis of the *S. hominis* plasmid.** The phylogenetic tree was constructed from the reference plasmid in **b)** and similar sequences retrieved from the NCBI plasmid database (criteria: ≥ 95% identity and ≥ 90% coverage). **d) Structural architecture of a resistance-carrying phage-plasmid.** Schematic diagram showing the co-localization of the biocide resistance genes *qacAB* and *qacR* on Plasmid 2, with homologous sequences also identified on Plasmid 1. The relative spatial orientation and genomic context of both plasmids within the phage-plasmid structure are illustrated.

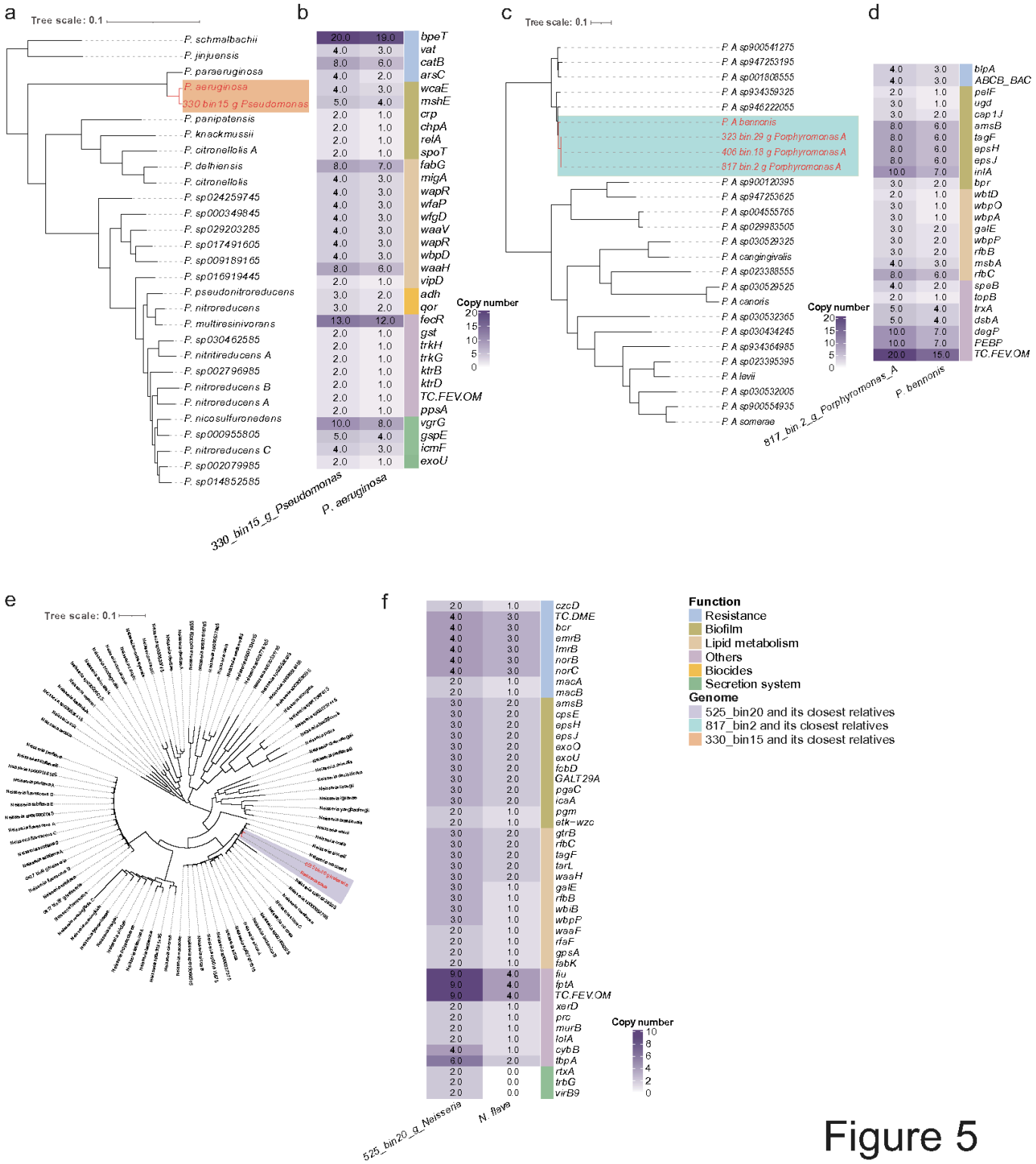


Figure 5

Figure 5

Comparative genomic analysis and functional gene expansion in novel ICU-associated taxa. a, c, e) Phylogenomic placement of novel rMAGs. Maximum-likelihood phylogenetic trees illustrating the evolutionary relationships of novel genomes belonging to genera **a)** *Pseudomonas* (330_bin.15), **c)** *Porphyromonas_A* (817_bin.2), and **e)** *Neisseria* (525_bin.20) alongside recognized species within their respective genera. **b, d, and f) Enrichment of specialized functional toolkits.** Comparative analysis of

gene copy number for functions of interest in the three novel taxa and their phylogenetically closest relatives. Only functional categories that exhibit significant expansion in the novel genomes relative to reference genomes are shown. Color intensity is proportional to the gene copy number, illustrating a specific pattern of gene duplication or expansion associated with adaptation to the clinical environment.

Supplementary Files

This is a list of supplementary files associated with this preprint. Click to download.

- TableS1.xlsx
- TableS2.xlsx
- TableS3.xlsx
- TableS4.xlsx
- FigureS1.eps
- FigureS2.eps
- FigureS3.eps
- FigureS4.eps
- FigureS5.eps